Journal of Nuclear Materials 403 (2010) 101–107

Contents lists available at ScienceDirect

Journal of Nuclear Materials

journal homepage: www.elsevier.com/locate/jnucmat

Preferential precipitation of hydrides in textured zircaloy-4 sheets

N.A.P. Kiran Kumar [a,*], Jerzy A. Szpunar [a], Zhang He [b]

[a] McGill University, 3610 University Street, Montreal, Quebec, Canada H3A 2B2
[b] Atomic Energy of Canada Limited, Chalk, River Laboratories, Ontario, Canada

ARTICLE INFO

Article history:
Received 6 April 2010
Accepted 1 June 2010

ABSTRACT

Cold-worked and stress relieved (CWSR) zircaloy-4 sheet-samples were charged with 45–247 wt. ppm of hydrogen using an electrolytic technique. Morphology and orientation of hydrides was examined with the help of optical microscopy (OM) and electron backscatter diffraction (EBSD) technique. The hydrides identified as δ-$ZrH_{1.5}$ phase by EBSD analysis, were located both within the grains and along the grain boundaries, but the grain boundary hydrides appeared to be dominant. The hydrides and the matrix have the (0 0 0 1)α-Zr//(1 1 1)δ-$ZrH_{1.5}$ orientation relationship at all locations. Three types of grain boundary hydrides were observed. A closer look on the grain boundary hydrides shows that the grain boundary hydrides are not exactly on the grain boundary; but very near the grain boundaries that follow the crystallographic relation (0 0 0 1)α-Zr//(1 1 1)δ-$ZrH_{1.5}$, only very few exceptions were recorded. The preferential sites for the grain boundary hydrides were basal planes of zirconium matrix located close to grain boundaries. Also, the hydrides shows strong {1 1 1} texture with maxima located at the same angle on the pole figure as the maxima of basal plane of α-zirconium matrix. The reproducibility of the results was verified using samples with different hydrogen concentrations.

1. Introduction

Zircaloy-4 is widely used as a key structural material (e.g., cladding material) of CANDU®[1] fuel-bundles. Hydrogen pick-up during fuel-bundle irradiation leads to formation of hydrides, often in the form of platelets in the material. These hydrides have a deleterious impact on the mechanical properties of the material. Thus an in-depth understanding of the hydriding process and the hydride orientation relative to the α-zirconium matrix should contribute to improvement in fuel-manufacturing technologies and may increase the safety margin.

It is well known that the hydrogen solubility in α-zirconium decreases rapidly from 6 at.% at 550 °C, to 0.7 at.% at 300 °C, and 10^{-4} at.% at room temperature [1] and that excess hydrogen is precipitated from the matrix in the form of zirconium hydrides. Three types of hydride phases were reported earlier and which one is formed depends on the cooling rate and hydrogen concentration. Among the hydrides, the literature about γ-hydride (FCT) is contradictory with two review articles reporting it as metastable [2,3] and others reported it as equilibrium phase below 250 °C [4,5], δ-hydride (FCC) is considered to be a stable phase that is formed during slow cooling and ε-hydride (FCT) is formed at higher hydrogen concentration (63 at.%) [2]. It is well known that the δ-hydride phase is most often formed in the material during bundle irradiation; however, there has been little discussions on formation mechanism of δ-hydrides [6,7].

It has been proposed that, in unstressed sample, hydrides would grow into grains along particular habit planes of the matrix [8,9]. Various habit planes have been suggested to date, like the prism plane of {1 0 $\bar{1}$ 0} [10,11], pyramidal plane of {1 0 $\bar{1}$ 1} [12,13], basal plane (0 0 0 1), {1 0 $\bar{1}$ 7}, [9,14] and twinning planes of {1 0 $\bar{1}$ 2}, {1 1 $\bar{2}$ 1} and {1 1 $\bar{2}$ 2} [15] of the HCP matrix. Insufficient evidence has been presented to support these assignments however, and the facts that many habit planes have been suggested make it difficult to understand the crystallographic relationship between the hydride and the matrix. A few researchers reported that the hydride preferential sites are grain boundaries (inter-granular hydrides) but could not come up with rationalized notations [16]. Few papers reported the crystallographic relation of inter-granular hydrides in zircaloy-2 [6,17–19]. Zircaloy-4 that has slightly higher iron content and almost no nickel is showing better resistance to hydrogen pick-up than zircaloy-2 [20,21]. However, the amount of hydrogen pick-up in the material increases with fuel irradiation time; and therefore a thorough understanding of hydride precipitation behavior in zircaloy-4 is needed for further improvement of fuel irradiation performance.

Zirconium hydrides at macroscopic level can be identified and tracked by neutron and X-ray diffraction techniques [22,23]. However for microscopic levels, where high spatial resolution characterization is needed, TEM and EBSD are used. For the present work EBSD was used over TEM, as it gives more statistically reliable data and allows obtaining information from larger areas [24].

* Corresponding author. Tel.: +1 514 398 4755.
E-mail address: anantha.nimishakavi@mail.mcgill.ca (N.A.P. Kiran Kumar).

[1] CANDU® is a registered trademark of Atomic Energy of Canada Limited (AECL).

0022-3115/$ - see front matter © 2010 Elsevier B.V. All rights reserved.
doi:10.1016/j.jnucmat.2010.06.005

The objective of the present investigation was to determine the crystallographic relationship between δ-hydrides and the matrix in zircaloy-4 CWSR sheet. Because zircaloy-4 sheet- and tubing-materials are both used for fabrication of CANDU fuel-bundles, and they have very similar texture and hydrogen pick-up behavior, the results of this investigation are also applicable to the tubing material.

2. Experimental

The chemical composition of the zircaloy-4 sheet-material is given in Table 1. The samples, provided by Atomic Energy of Canada Limited (AECL), were electrolytically hydrided in 0.125 M H_2SO_4 solution at AECL Chalk River Laboratories. The current density was 150 mA/cm^2, and the solution temperature was controlled at 70 ± 5 °C. Hydrogen content in the samples was varied from 45 wt. ppm to 247 wt. ppm by adjusting the operation time for the hydrogen-charge process. After the charging, the samples were homogenized by heating them in flowing argon at 375 °C for 3 h, and then furnace cooling to room temperature. The hydrogen concentrations in the samples were determined by hot vacuum extraction mass spectrometry.

Table 1
Alloy composition of zircaloy-4.

Zircaloy-4	Sn (wt.%)	Fe (wt.%)	Cr (wt.%)	Ni (wt.%)	O (wt.%)	Zr (wt.%)
	1.52	0.21	0.11	<35 ppm	0.125	Bal

The samples for EBSD analysis were prepared by etching them in a solution of 45% HNO_3, 45% H_2O and 10% HF, followed by colloidal silica polishing. The EBSD measurements were carried out with an orientation imaging microscopy (OIM) system, installed on a FEG XL30 scanning electron microscope (SEM). The EBSD patterns were obtained and analyzed by means of the TSL OIM software.

2.1. The reference frame for electron backscatter pattern (EBSP) analysis

The zircaloy-4 sheet directions represented in the present optical, EBSD and texture analyses are RD, TD and ND. Where RD is the rolling direction of the sheet, TD is the transverse direction of the sheet and ND is the normal direction.

3. Results and discussions

3.1. Optical microscopy

Optical examination of the hydrided samples revealed the presence of hydride platelets. Many hydride platelets found to be precipitated in the direction perpendicular to applied stress in ND–TD, ND–RD, RD–TD planes in the form of longs chains as shown in Fig. 1.The grains and grain boundaries are however not discernable optically, and thus, we cannot obtain any detailed information regarding location of the hydrides with respect to the grains and grain boundaries. However, this information is crucial for understanding the mechanical behavior of the material, for example, fracture mechanism of it under load.

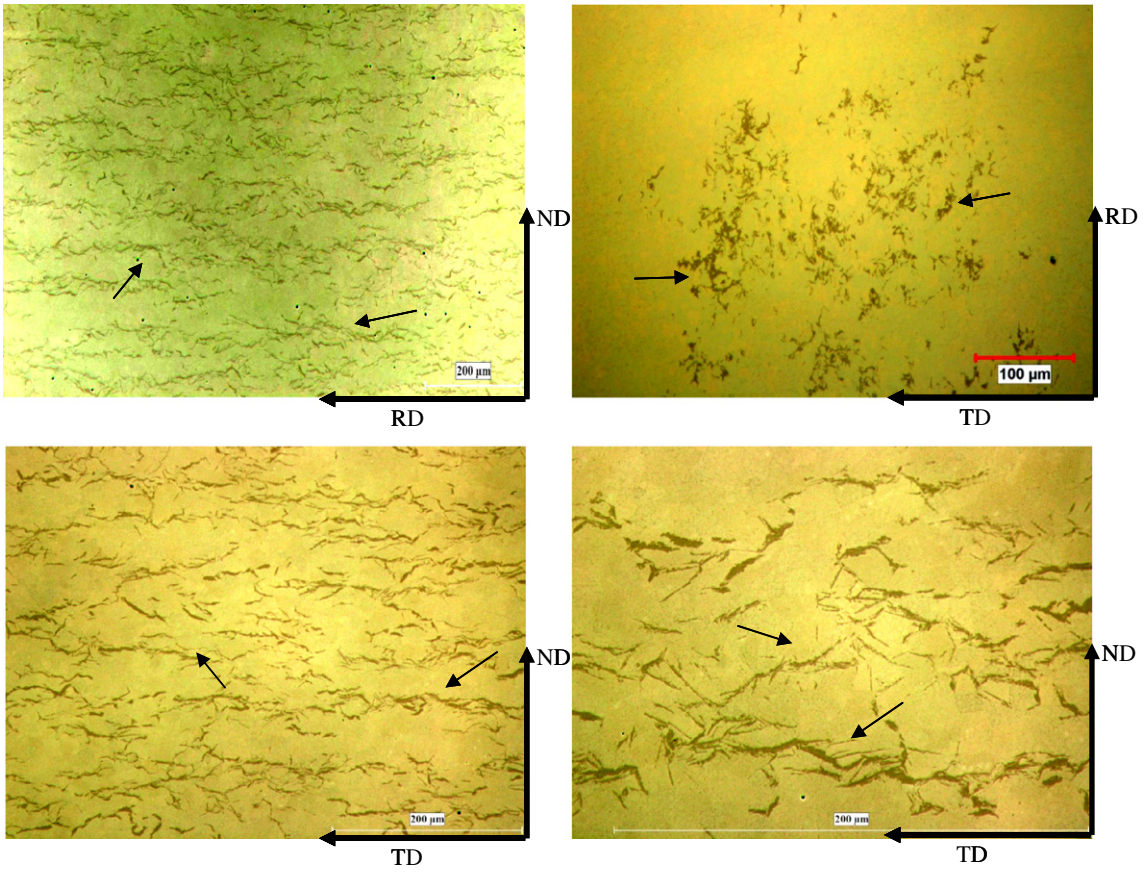

Fig. 1. Typical optical micrographs of the samples with ~247 wt. ppm of hydrogen. Note the hydrides (arrow) are along the TD direction in ND–TD planes; along RD direction in ND–RD planes and along RD direction in RD–TD planes.

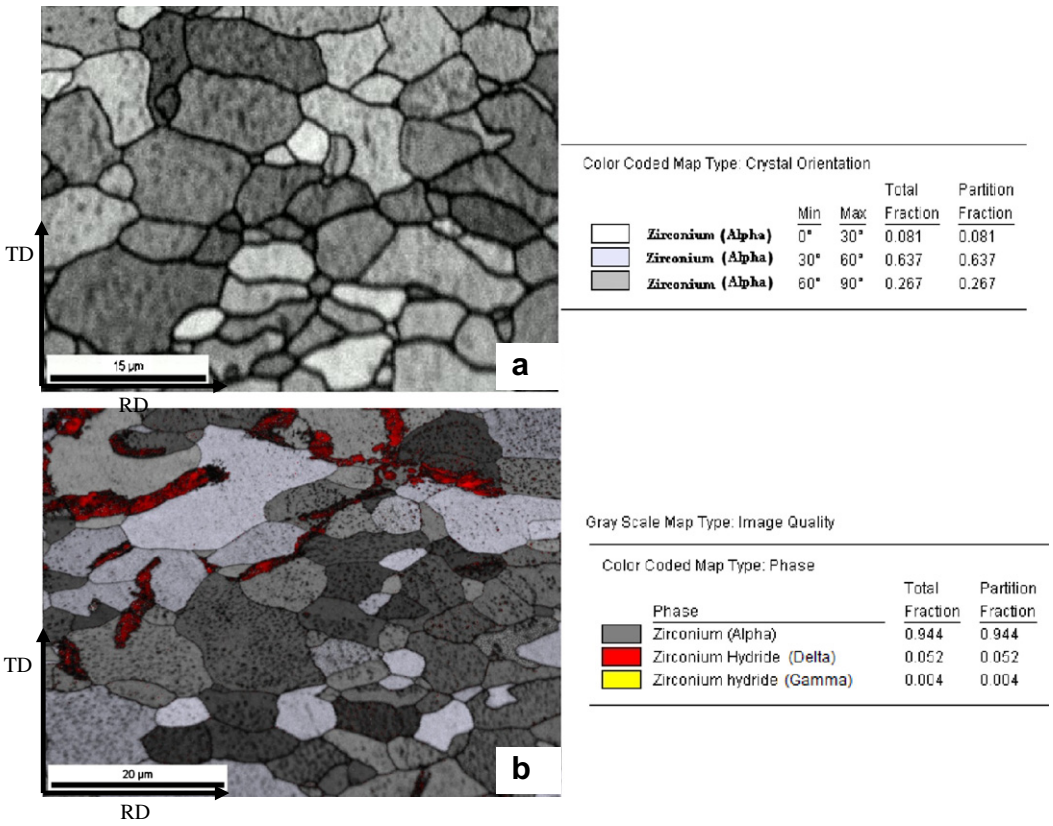

Fig. 2. EBSD grain and phase map of: (a) un-hydrided and (b) hydrided zircaloy-4 samples (247 wt. ppm).

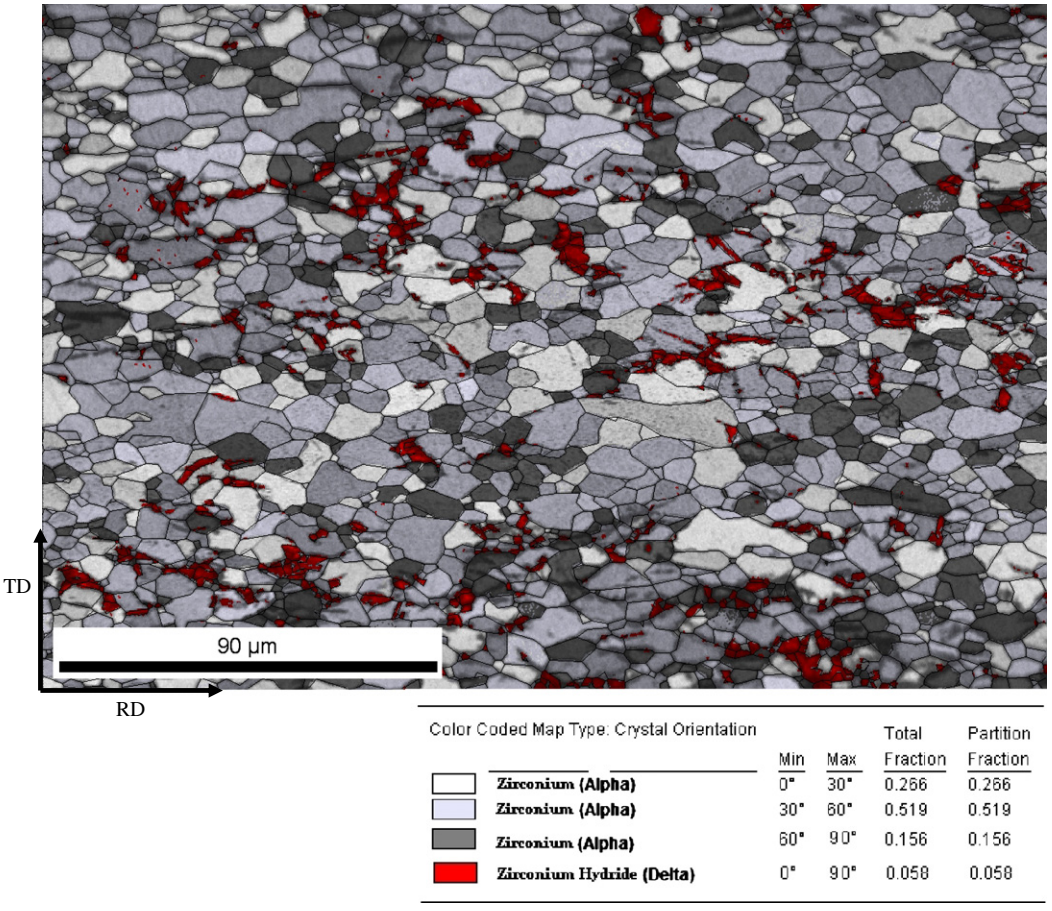

Fig. 3. EBSD grain map of hydrided sample at lower magnification (247 wt. ppm).

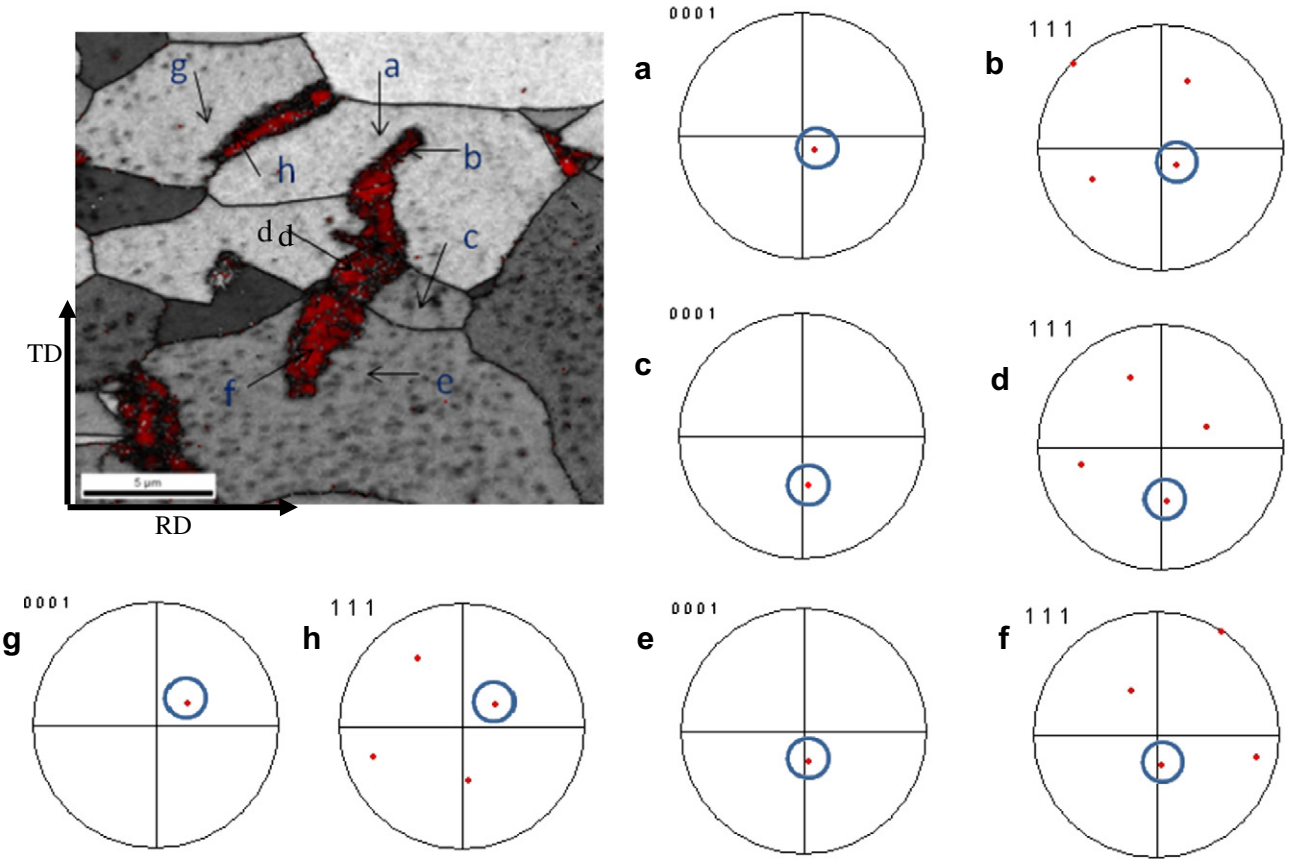

Fig. 4. Zirconium hydrides precipitated within grains and at grain boundaries.

3.2. Hydride crystallographic orientation

The EBSD technique not only identifies the hydride phase by indexing their characteristic diffraction patterns, but also determines their crystallographic orientations with respect to zircaloy-4 matrix. Kikuchi patterns indexed with EBSD system show the presence of α-zirconium (HCP) and δ-hydrides (FCC), with negligible amount of γ-hydride. Fig. 3 shows the grain map of un-hydrided and hydrided samples where each grain is mapped with different color code based on the crystal orientation. As shown in Fig. 2a, the matrix has the characteristic CWSR microstructure characterized by the presence of elongated grains along the rolling direction (RD). Fig. 2b shows the typical microstructure of hydrided sample. For better contrast, the hydrides are marked with red[2] color.

The α-zirconium (HCP) matrix and δ-$ZrH_{1.5}$ (FCC) hydrides are indentified using the standard Kikuchi patterns of zirconium (JCPDS-00-005-0665) and zirconium hydride (JCPDS-00-008-0218), respectively. As shown in Fig. 2, the hydrides have precipitated both inside the grains and along the grain boundaries. EBSD was also recorded at lower magnification as shown in Fig. 3, in-order to obtain good statistical data about the hydride precipitation sites.

Out of 150 analyzed locations 97 were observed to be grain boundary hydrides, where as 53 were intra-granular (within the grains) hydrides. So the ratio of intra-granular hydrides to inter-granular hydrides is about 1.8 which indicates that hydride precipitation along the grain boundaries is predominant. However, the ratio of inter-/intra-granular hydrides varies based on the cooling rate and initial sample condition [17,25,26].

3.2.1. Intra- and Inter-granular hydrides

In the literature [27,28] different habit planes were suggested for intra-granular hydrides. To determine the habit plane for the present samples, the crystallographic relationship between the hydrides and the α-zirconium matrix was analyzed using pole figure method. The hydrides were observed within the grains, although they are in contact with the grain boundaries along its length. At all points intra- and inter-granular hydrides were found following $(0\,0\,0\,1)\alpha\text{-}Zr//(1\,1\,1)\delta\text{-}ZrH_{1.5}$ relationship as illustrated in Fig. 4. This observation supports the interpretation of hydride formation proposed by Une et al. [13,29] for zircaloy-2 samples and such orientation relationship exists in the alpha component of Zr–2.5 wt.%Nb alloy as well [18]. Root et al. [4] have also shown by neutron diffraction that such orientation relationship exists for both δ- and γ-hydrides.

3.2.2. Hydride at grain boundaries

Three types of grain boundary hydrides were observed in the stress relieved zircaloy-4 samples.

(1) Hydride initiated at the grain boundary, but growing on both sides of the grain as shown in Fig. 5I.
(2) Hydride along the grain boundary; on both sides of the grain boundary as shown in Fig. 5II.
(3) Hydride near the grain boundary as shown in Fig. 5III.

These three types of grain boundary hydrides look like precipitates on the grain boundary at lower magnification in EBSD and

[2] For interpretation of color in Figs. 1–8, the reader is referred to the web version of this article.

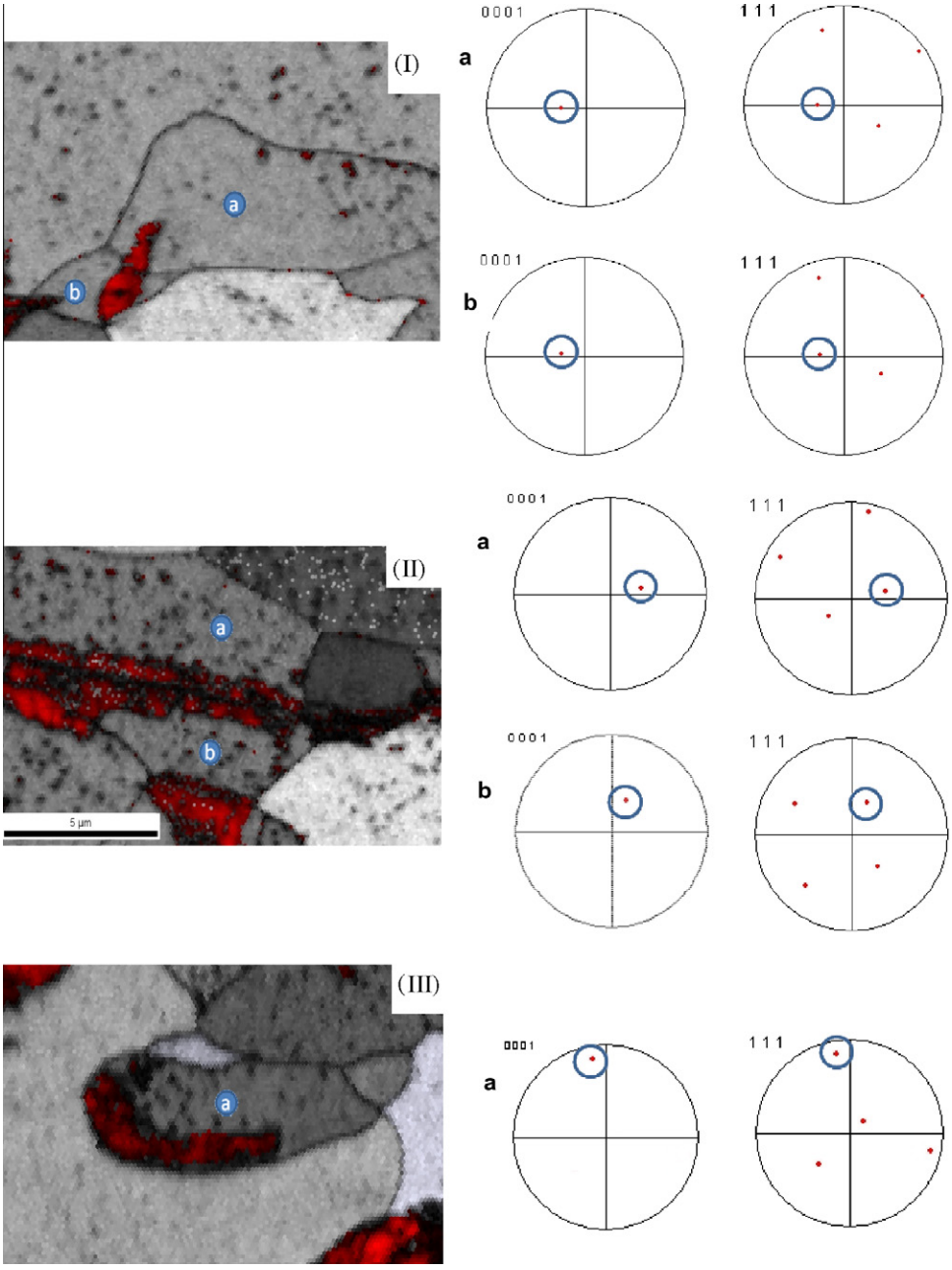

Fig. 5. Three different grain boundary hydride. Hydrides growing: (I) on both sides of the grain boundary, (II) on the grain boundary and (III) near the grain boundary.

optical micrographs. But this observation can be misleading. Let us look at the grain boundary hydrides at higher magnification in-order to get a clear picture on the hydride orientation relation with the zirconium matrix.

3.2.2.1. Hydride growing on both sides of the grain boundary. In this case the hydride on the grain "a" is found to be following the $(0\,0\,0\,1)\alpha$-Zr//$(1\,1\,1)\delta$-$ZrH_{1.5}$ orientation relation with the grain "a" and the hydride on grain "b" is found to be following the $(0\,0\,0\,1)\alpha$-Zr//$(1\,1\,1)\delta$-$ZrH_{1.5}$ orientation relation with the grain "b".

3.2.2.2. Hydride on the grain boundary. In this case hydride precipitated at the grain boundary. But even here the hydride near to the grain boundary on the grain "a" is showing $(0\,0\,0\,1)\alpha$-Zr//$(1\,1\,1)\delta$-$ZrH_{1.5}$ orientation relationship and the hydride on the grain "b" near the grain boundary is again following $(0\,0\,0\,1)\alpha$-Zr//$(1\,1\,1)\delta$-$ZrH_{1.5}$ orientation relationship with the zirconium matrix.

3.2.2.3. Hydride near the grain boundary. This is the most interesting case; unlike in the above two cases, the hydride is growing within a single grain without spreading onto other grains, however also in this case $(0\,0\,0\,1)\alpha$-Zr//$(1\,1\,1)\delta$-$ZrH_{1.5}$ orientation relationship is clearly observed.

A closer look at the grain boundary hydrides shows that the hydrides are very close to the grain boundaries following $(0\,0\,0\,1)\alpha$-Zr//$(1\,1\,1)\delta$-$ZrH_{1.5}$ orientation relationship.

The hydride, during the fast cooling, may precipitate at random grain boundaries, but in the case of δ-hydrides which forms at slow cooling rates and also mainly observed during nuclear reactor operation are found to be showing crystallographic relation with the zirconium matrix. The hydride precipitation is reported to be

associated with micro stresses which arise from cold working [30]. But this is ruled out in the present case as the sample is stress relieved. Perhaps the most revealing part of the presented analysis is that, in-order to follow $(0\,0\,0\,1)\alpha\text{-Zr}//(1\,1\,1)\delta\text{-ZrH}_{1.5}$ orientation relationship with zirconium matrix, the hydrides are precipitating on the grains whose basal planes is oriented close to the grain boundary. In this way, the elastic strain energy and interferential energy and at the same time grain boundary energy can be minimized. Singh et al. using strain energy minimization technique, has reported that δ-hydride can minimized its strain energy by precipitating on basal plane $(0\,0\,0\,1)$ of α-zirconium [31]. This preferential behavior of δ-hydrides can be a reason for inhomogeneous precipitation of hydrides at different parts of the sample.

3.3. Sample with low hydrogen concentration

Experiments were performed on the sample with 117 wt. ppm hydrogen. Fig. 6 shows a typical EBSD pattern of sample. A lower number of small hydride platelets is recorded however even in this case the hydrides still followed the $(0\,0\,0\,1)\alpha\text{-Zr}//(1\,1\,1)\delta\text{-ZrH}_{1.5}$ orientation relation, irrespective of the hydride location.

3.4. Texture

The micro and macro texture data were obtained from X-ray diffraction (XRD) and EBSD techniques, respectively. Both shows strong $(0\,0\,0\,2)$ basal plane texture, a typical texture of CWSR zircaloy-4 material as shown in Fig. 8.

Interestingly, both the micro and macro texture analyses of the hydride phase show that the zirconium hydride has a strong {1 1 1} texture and if we compare the results presented in the pole figures of Figs. 7 and 8, we can find that, the peak of basal plane of zirconium and the {1 1 1} plane of zirconium hydride are at the same location (i.e., the areas color-coded in red in the pole figures). This implies that {1 1 1} plane of zirconium hydrides always prefer to orient parallel to the $(0\,0\,0\,2)$ basal plane of the matrix.

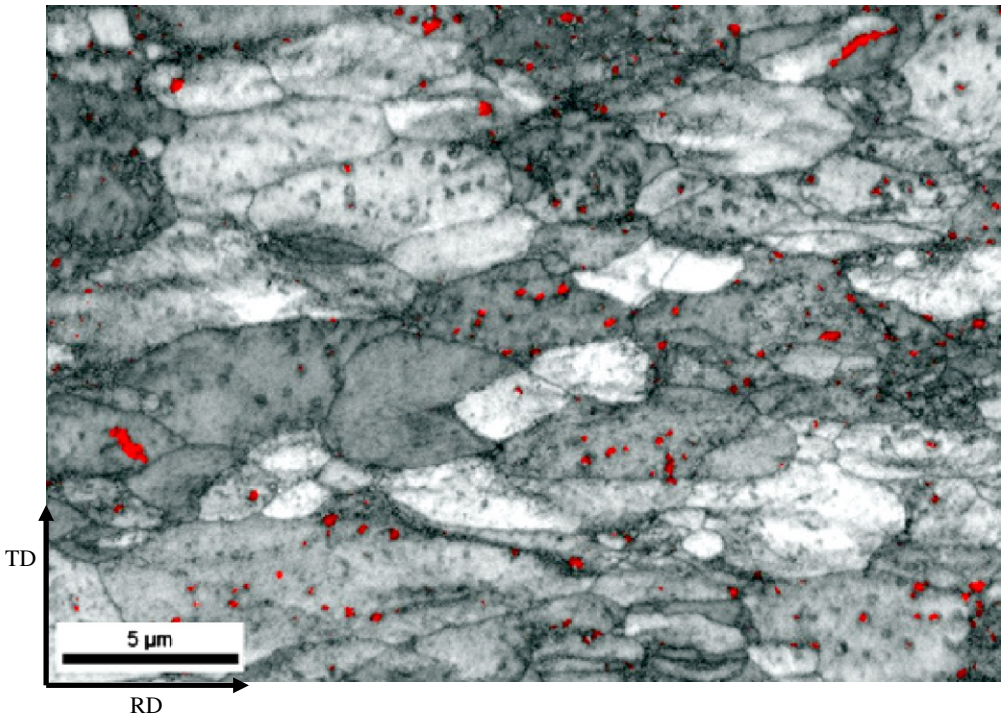

Fig. 6. EBSD of sample with 117 wt. ppm hydrogen concentration.

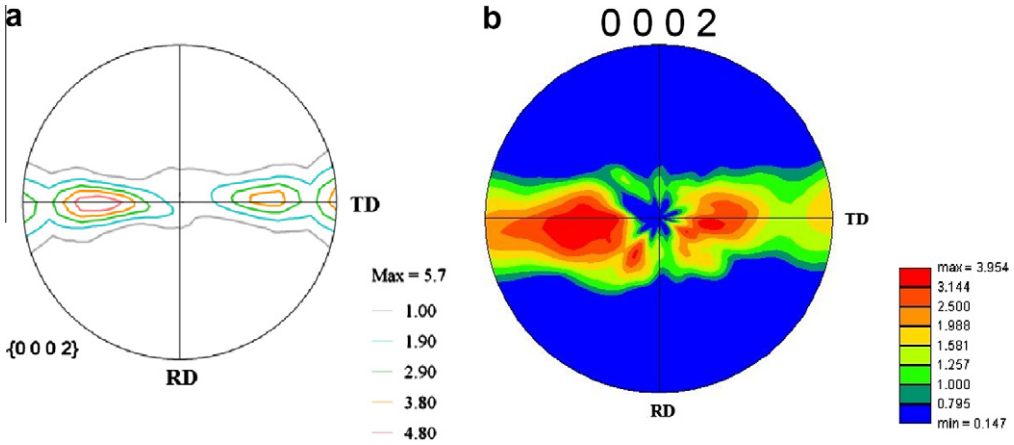

Fig. 7. $(0\,0\,0\,2)$ Basal plane texture of zircaloy-4 sheet: (a) macro texture determined by XRD and (b) micro texture determined by EBSD.

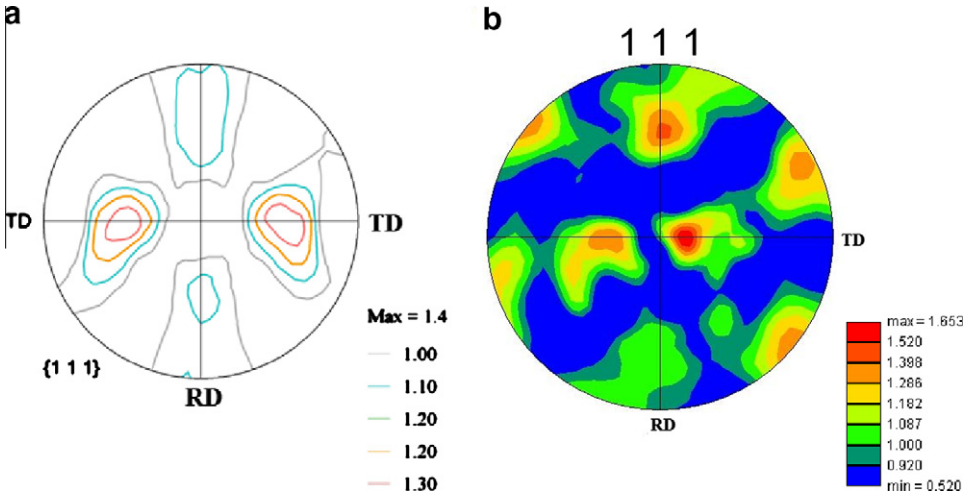

Fig. 8. Texture of zirconium hydride (δ-$ZrH_{1.5}$): (a) macro texture and (b) micro texture.

The present study provides the detailed evidence about grain boundary hydrides and documents the orientation relationship of hydrides with the zirconium matrix in CWSR zircaloy-4 samples.

4. Conclusions

The Crystallographic orientation between the hydrides and a CWSR zircaloy-4 matrix was examined using the EBSD technique. The following conclusions can be derived based on the results of this investigation:

1. Statistical data on hydrided sample (247 wt. ppm) shows more inter-granular hydrides than intra-granular hydrides in CWSR zircaloy-4 sheet.
2. Both inter-granular and intra-granular hydride are found to follow the (0 0 0 1)α-Zr//(1 1 1)δ-$ZrH_{1.5}$ orientation relationship with the zirconium matrix.
3. Three types of grain boundary hydrides were observed. EBSD at higher magnification shows that hydrides are very close to the grain boundaries following (0 0 0 1)α-Zr//(1 1 1)δ-$ZrH_{1.5}$ orientation relationship.
4. Hydride preferential site are the grains that have basal plane close to the grain boundaries and decreasing hydrogen concentration has no effect on the (0 0 0 1)α-Zr//(1 1 1)δ-$ZrH_{1.5}$ orientation relationship.

Acknowledgement

Authors would like to thank Natural Sciences and Engineering Research Council of Canada (NSERC) for supporting this project.

References

[1] J.J. Kearns, J. Nucl. Mater. 22 (3) (1967) 292–303.
[2] D.O. Northwood, U. Kosasih, Int. Met. Rev. 28 (2) (1983) 92–121.
[3] L. Lanzani, M. Ruch, J. Nucl. Mater. 324 (2–3) (2004) 165–176.
[4] J.H. Root, W.M. Small, D. Khatamian, O.T. Woo, Acta Mater. 51 (7) (2003) 2041–2053.
[5] S. Mishra, K.S. Sivaramakrishnan, M.K. Asundi, J. Nucl. Mater. 45 (3) (1972) 235–244.
[6] M.P. Cassidy, C.M. Wayman, Metall. Mater. Trans. A 11 (1) (1980) 47–56.
[7] S.S. Sidhu, N.S. Satya Murthy, Adv. Chem. 39 (1963) 87–98 (Chapter 8).
[8] V.S. Arunachalam, B. Lehtinen, G. Ostberg, J. Nucl. Mater. 21 (3) (1967) 241–248.
[9] D.G. Westlake, J. Nucl. Mater. 26 (2) (1968) 208–216.
[10] J.E. Bailey, Acta Metall. 11 (4) (1963) 267–280.
[11] Y. Lium, Q. Peng, W. Zhao, H. Jiang, Mater. Chem. Phys. 110 (1) (2008) 56–60.
[12] H.M. Chung, R.S. Daum, J.M. Hiller, M.C. Billone, Characteristics of hydride precipitation and reorientation in spent-fuel cladding, zirconium in the nuclear industry, in: 13th International Symposium, ASTM STP, vol. 1423, 2002, pp. 561.
[13] K. Une, S. Ishimoto, J. Nucl. Mater. 389 (3) (2009) 436–442.
[14] C. Roy, J.G. Jacques, J. Nucl. Mater. 31 (2) (1969) 233–237.
[15] F.W. Kunz, A.E. Bibb, Trans. Metall. Soc. AIME 218 (1960) 133.
[16] R.P. Marshall, J. Nucl. Mater. 24 (1) (1967) 34–48.
[17] C.E. Ells, J. Nucl. Mater. 28 (2) (1968) 129–151.
[18] V. Perovic, G.C. Weatherly, C.J. Simpson, Acta Metall. 31 (9) (1983) 1381–1391.
[19] D.G. Westlake, J. Nucl. Mater. 16 (2) (1965) 215–219.
[20] P.A. Schweitzer, Corrosion Engineering Hand Book, Marcel Dekker, Inc., 1996 (July).
[21] W.K. Anderson, M.J. McGoff, Corrosion of zircaloy in crevices under nucleate boiling conditions, Technical Report, Knolls Atomic Power Lab, Schenectady, NY, 1962.
[22] J.H. Root, R.W.L. Fong, J. Nucl. Mater. 232 (1) (1996) 75–85.
[23] W.M. Small, J.H. Root, D. Khatamian, J. Nucl. Mater. 256 (2–3) (1998) 102–107.
[24] A.F. Gourgues, Mater. Sci. Technol. 18 (2) (2002) 119–133.
[25] B. Nath, G.W. Lorimer, N. Ridley, J. Nucl. Mater. 49 (3) (1973) 262–280.
[26] B. Nath, G.W. Lorimer, N. Ridley, J. Nucl. Mater. 58 (2) (1975) 153–162.
[27] K. Une, Kazuhiro Nogita, J. Nucl. Sci. Technol. 41 (7) (2004) 731–740.
[28] J.S. Bradbrook, G.W. Lorimer, N. Ridley, J. Nucl. Mater. 42 (2) (1972) 142–160.
[29] K. Une, S. Ishimoto, J. Nucl. Mater. 357 (1–3) (2006) 147–155.
[30] K.V. Mani Krishna, A. Sain, I. Samajdar, Acta Mater. 54 (18) (2006) 4665–4675.
[31] R.N. Singh, P. Stahle, L.b. Sills, M. Ristmanna, S. Banerjee, Defect Diffus. Forum 279 (1) (2008) 105–110.